

PAH structure analysis of soot in a non-premixed flame using High-Resolution Transmission Electron Microscopy and Optical Band Gap Analysis

Maria Botero¹, Erin M. Adkins², Silvia González Calera¹, Houston Miller²,
Markus Kraft^{1,3}

released: 19 March

¹ Department of Chemical Engineering
and Biotechnology
University of Cambridge
New Museums Site
Pembroke Street
Cambridge, CB2 3RA
United Kingdom
E-mail: mk306@cam.ac.uk

² Department of Chemistry
George Washington University
Corcoran Hall
725 21st St. NW
Washington, DC 20052
USA

³ School of Chemical and Biomedical Engineer-
ing
Nanyang Technological University
62 Nanyang Drive
6357459
Singapore

Preprint No. 156



Keywords: soot, laser extinction, optical band gap, HRTEM, lattice-fringe analysis

Edited by

Computational Modelling Group
Department of Chemical Engineering and Biotechnology
University of Cambridge
New Museums Site
Pembroke Street
Cambridge CB2 3RA
United Kingdom

Fax: + 44 (0)1223 334796

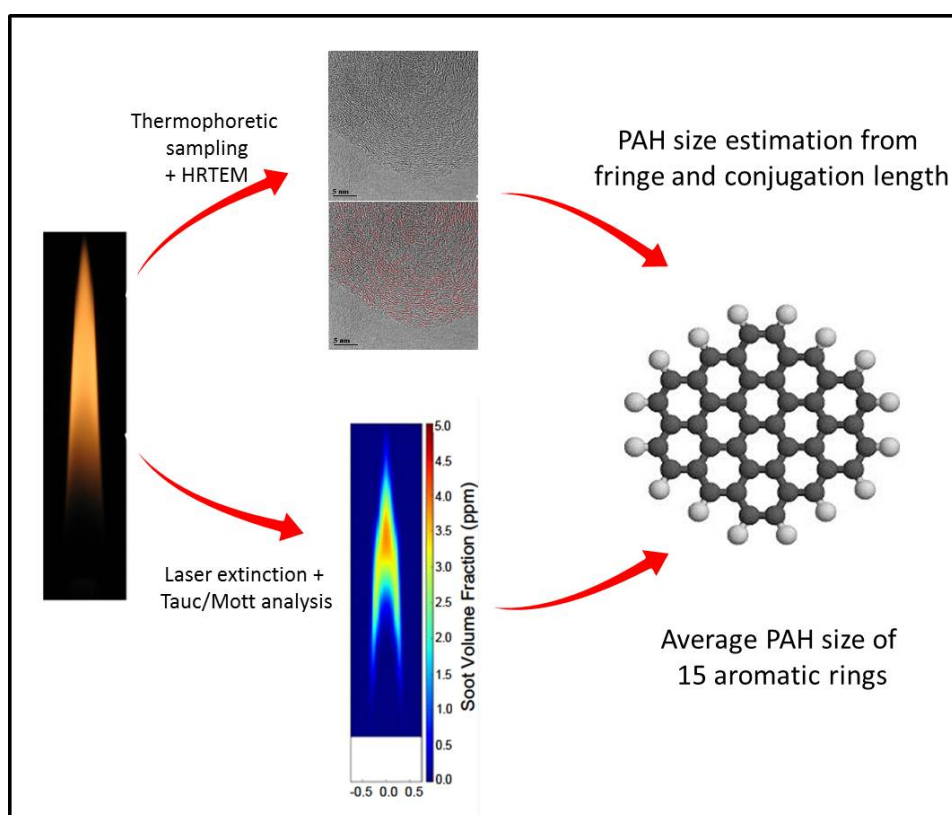
E-Mail: c4e@cam.ac.uk

World Wide Web: <http://como.cheng.cam.ac.uk/>



Abstract

Soot particles formed in a system of non-premixed liquid fuel flames supported on a wick-fed, smoke point test burner (ASTM D1322-08) were characterised by in-situ visible light extinction and thermophoretically-sampled high-resolution transmission electron microscopy measurements, HRTEM. The fuels studied were heptane, toluene and their iso-volumetric mixture (H50T50), given their relevance as surrogate fuels. Extinction measurements were used to calculate the soot volume fraction, F_V , and determine the optical band gap (OBG) as a function of flame position. The OBG was derived from the near-edge absorption feature using Tauc/Davis-Mott analysis. For the HRTEM analysis, soot samples were collected at different locations in the flame using thermophoretic sampling and a fast-insertion technique. The images were then analysed using a ‘lattice-fringe’ algorithm, to determine important parameters such as the fringe length. Polycyclic aromatic hydrocarbon (PAH) sizes were estimated from conjugation length obtained from OBG measurements and fringe lengths from HRTEM measurements. Across all studied flames, the peak F_V ranged from 3.8 ppm in the heptane flame to 18.0 ppm in the toluene flame. Despite this wide range, the average OBG across the different flames only varied from 1.99 eV in the H50T50 to 2.06 eV in the heptane flames, which is consistent with molecule lengths of between 0.98 nm and 1.02 nm. Lattice fringe analysis yielded slightly lower average fringe lengths between 0.85 - 0.96 nm throughout the different flames. This work provides experimental support to the model of soot formation where the transition from chemical to physical growth starts at a modest molecular size; about the size of circumpyrene.



1 Introduction

The high complexity of petroleum-based fuels has encouraged the search for mixtures of limited components to ease the development of new combustion technologies through computational tools, and to generate insight and understanding of underlying fundamental processes. Commercial fuels are mixtures of hundreds of hydrocarbons. The primary chemical classes of hydrocarbons in fuels are paraffins, olefins and aromatics [22, 42]. The soot particles formed by the combustion of these fuels are widely regarded as pollutants, and are increasingly regulated both in terms of number and mass of particulate matter emitted from on-road vehicles.

Sooting limits are defined to assess the sooting propensity of a fuel. In co-flow diffusion flames a common target is the smoke point - the greatest flame height without smoke emission under laminar diffusion combustion [6]. A lower smoke point indicates a higher sooting tendency. In 1950's the first studies trying to relate the molecular structure of hydrocarbons with smoke point were published [31, 49]. The results indicated that the rate at which hydrocarbons produced soot increased as follows: paraffins < isoparaffins < mono-olefins < naphthenes < alkynes < aromatics. The more compact the structure, the greater the tendency to soot. Further, several studies have observed that a high percentage of fuel carbon in aromatic structures is converted into soot [28]. Therefore branched or cyclic structures present lower smoke points, although the effect is small compared with the increase in sooting tendency derived from the increase of aromatic character [10].

The formation of soot during combustion has been the subject of extensive research. The last century has seen significant efforts to explain model, and predict the hundreds of chemical and physical changes that take place in combustion processes [13, 25, 26, 39, 40, 43, 45, 53]. A widely accepted interpretation is that the pathway begins with the formation of molecular precursors such as polyacetylenes and polycyclic aromatic hydrocarbons (PAHs) from the fuel source [25]. There is some agreement that the rate limiting reaction is the formation of the first aromatic ring, for which various mechanisms have been proposed [5, 56]. The mechanism for particle inception is debated, but one model asserts that it occurs with the polymerisation of PAHs. As the molecular mass of PAHs increase a collision between two such molecules becomes more likely to result in the formation of a dimer [25]. Therefore polymerisation occurs at an increasing rate, forming larger molecules until the inception of a solid nucleus occurs. Another model for particle inception states that changes in temperature and pressure along the space result in condensation of PAHs, followed by formation of liquid nuclei, which then proceed to form solid particles [25, 56]. Once primary particles are formed, these nascent soot particles undergo surface growth (and in some systems, competing oxidation reactions), and the small particles agglomerate into larger fractal structures [25, 26, 37].

Experimental studies of soot morphology revealed that the crystallinity in mature soot particles arises due to stacking of planar PAHs to form parallel atomic layers and their alignment along the periphery of soot particles [18, 32, 54, 55]. It is clear from these studies that PAH molecules act as a soot precursor, and their relative orientations decide the crystalline (graphite-like) or amorphous nature of soot particles. The variations in the structure of the PAHs, their sizes and their orientations in soot particles has also been found to depend heavily on the type of the fuel producing it, fuel flow rate and the tem-

perature [2, 3]. The presence of PAH stacks and clusters revealed by HRTEM images of soot particles, indicates that the coagulation of PAHs may be responsible for soot nucleation. Furthermore, through Raman spectroscopy, crystallite sizes between 1.0-1.2 nm were estimated in a diffusion flame, corresponding to PAHs with 4-5 aromatic rings across (approximately the size of circumcoronene)[30].

In soot models it is often assumed that pyrene dimerisation is the critical soot particle formation step [12, 51]. However, there are a number of recent studies that challenge this view [5, 15, 16, 29, 50]. For example, the PAH growth mechanism presented by Violi [21] models large, non-planar PAH sheets in a flame-like environment. A large set of reactions describe the growth of a PAH molecule using a kinetic Monte Carlo (KMC) algorithm and Molecular dynamics (MD) techniques. They found that molecular size was the largest factor with the onset of dimerisation possibly beginning with PAHs the size of ovalene (C₃₈H₁₄) [21, 36]. Similar results were found in our group by employing a population balance PAH-PP (polyaromatic hydrocarbon-primary particle) model [14, 44, 48] coupled with KMC-ARS (kinetic Monte-Carlo-aromatic site). For the physical binding of PAHs based on van der Waals interactions large PAH molecules of the order of 50 carbon atoms were found to be required [27, 44]. Using conventional molecular dynamics (MD) simulations with the isoPAHAP potential (isotropic potential for the PAH interactions), the melting points of clusters of ovalene, hexabenzocoronene and circumcoronene were estimated. It was concluded that at 1500 K a critical size of peri-condensed PAH for a nascent soot particle is C₇₁H₂₁ and for a mature particle is C₅₄H₁₈ (circumcoronene) [17].

The purpose of this paper is to estimate the size of agglomerating aromatics in soot particles. A combination of two techniques is used to find characteristic lengths of PAHs: an optical band gap (OBG) determination from Tauc/Davis-Mott analysis [1] to estimate the conjugation length, and 'lattice-fringe' analysis from HRTEM images to estimate fringe lengths. We compare the results of the two techniques from soot formed in a wick-fed diffusion flame burning different liquid fuels. The fuels studied were heptane, toluene and their iso-volumetric mixture (H50T50), given their relevance as surrogate fuels. . Extinction measurements were used to calculate the soot volume fraction, F_v , and determine the OBG. Soot was thermophoretically sampled from the flames and imaged with HRTEM.

2 Methods

2.1 Burner

In this study, the smoke point test burner [6] was used as simple, known and standardised way to test different liquid fuels in terms of their combustion at atmospheric conditions. This wick-fed burner (inset **Figure 1**), that has been previously described [7, 57], was used to generate a laminar diffusion flame of liquid fuel. The burner consists of a cylindrical reservoir, with an inner concentric hole where the wick is placed, and a 7 mm i.d nozzle. The flame height is adjusted by rotating a threaded fitting and increasing the wick exposure (i.e, increasing the fuel flow rate).

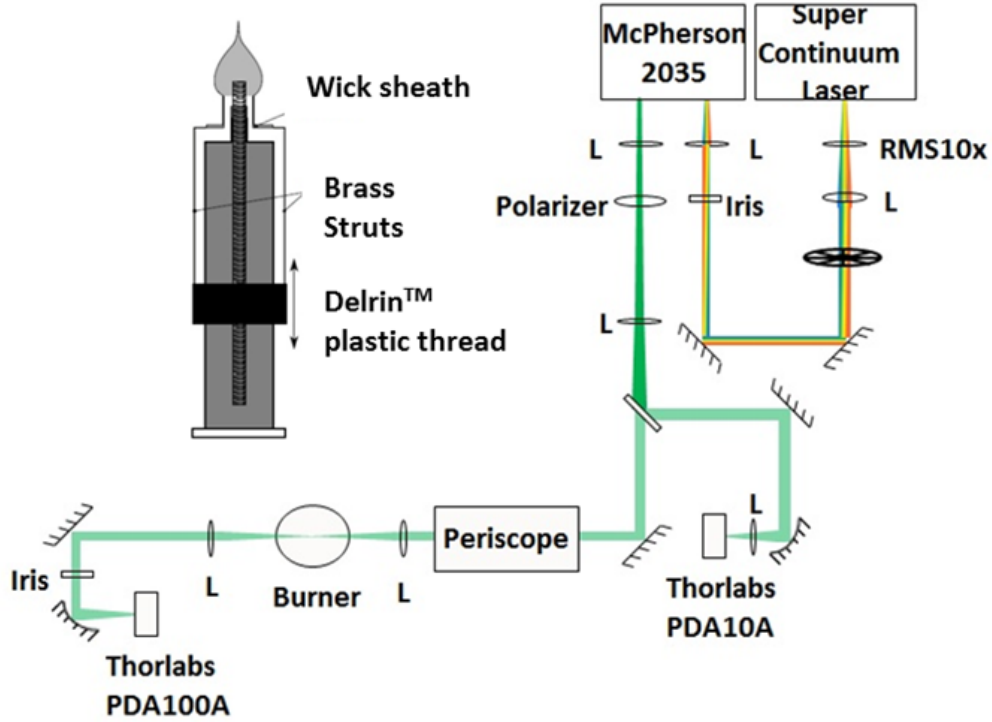


Figure 1: *Experimental schematic of line of sight extinction measurements (inset burner schematics).*

The fuels tested are heptane, toluene and their mixture of 50/50% by volume (H50T50). Flame heights close to the smoke point were selected: 4 cm, 0.7 cm and 1.1 cm respectively. In the case of heptane the selected flame height was much lower than its smoke point (7.3 cm) due to experimental limitations [7].

2.2 Extinction Measurements and Tauc analysis

The experiment schematic is shown in **Figure 1**. Full details of this set-up can be found in a previous manuscript [1]. In summary, the collimated beam from a broadband super continuum light source (NKT Photonics EXB-4) was expanded and focused onto the entrance slit of a monochromator, McPherson Model 2035 with 1200 g/mm gratings blazed at 500 nm (providing 2 nm resolution in the experimental configuration). The beam was then split into two channels, the extinction channel, which provided line of sight measurements through the flame and a power metering channel, which bypasses the flame allowing for power fluctuation monitoring. The transmitted light channel was periscoped into the flame and then focused into the centre of the flame, at the focal point the beam diameter was 0.47 mm. Downstream of the flame, the beam was collimated and focused onto a photodiode detector with a mounted diffuser facilitating detection. A pair of lock-in amplifiers, referencing a chopper at 400 Hz, were used to collect and digitise the signal.

The flame was horizontally scanned horizontally over the range -1.0 cm to 1.0 cm in 0.05 cm increments, at each wavelength. After completing the scan, the positioner would

return to the starting position and the monochromator would move 2 nm to the next wavelength. The procedure was repeated until the entire spectral range, 440 nm to 740 nm, was covered. The spectral range between 540 nm and 740 nm was covered with steps of 10 nm. The height above the burner (HAB) was measured from the burner rim. Heptane flame was mapped from a HAB of 0.5 cm in 0.5 cm increments until the tip (4 cm). H50T50 and toluene flames were mapped from 0.3 cm HAB, in increments of 0.2 cm until the flame tip (1.1 cm and 0.7 cm respectively).

Given that the flame is axi-symmetric, the line of sight extinction will be a combination of contributions from the different radial positions. The radially distributed extinction was tomographically reconstructed using an Abel inversion technique. In this work, the extinction spectra as a function of wavelength are fit to an exponential function prior to tomographic reconstruction to prevent degradation in the signal-to-noise ratio. Fitting the spectra prior to inversion also allows for the quantification of the noise in such a way that the error can be propagated to determine the uncertainty this noise causes in the OBG determination. In addition to quantifying the noise in the data set, the uncertainty is quantified by calculating the deviation in replicate experiments at HAB 2 cm, 0.7 cm and 0.5 cm for heptane, H50T50 and toluene experiments, respectively. The reported error in the OBG is the sum of the uncertainty from calculating the extinction on replicate runs and the error propagated from the exponential fit.

2.3 HRTEM and fringe-lattice analysis

Soot particles are driven thermophoretically to the cold wall of the probe and are ultimately captured on its surface [20]. A fast insertion technique is used to protect the grid from thermal damage [33]. The soot particles were collected in holey carbon films on 300 mesh cooper grids. Samples were collected at different position in the flames. Heptane flame was sampled along the centerline at 1 cm, 2 cm, 3 cm, and 4 cm HAB, and at the flame front at 1 cm and 2 cm HAB. Due to the small size of H50T50 and toluene flames, samples were taken at only at 0.7 cm and 1.1 cm HAB and 0.7 cm HAB, respectively.

TEM images were taken using a JEOL 3011 microscope with a specified point-to-point resolution of 0.17 nm. The operating voltage of the microscope is 300 keV using a Lab6 filament. Gatan image software v.3.4 was used for microscope operation. At least 10 images acquired in different regions of the grid (5-10 squares surrounding the grid centre) obtained at different magnifications (500,000 and 600,000) were selected for image analysis.

The HRTEM image analysis algorithm used here was developed and implemented using MATLAB (The Math Works Inc., Natick, MA) based on literature approaches [60], without relying upon commercial image processing packages with unknown preset parameters. A full description of the algorithm can be found in [8]. The processing technique of HRTEM images involves several steps. In general, the background noise is filtered at the Fourier transform level using different bandpass filters. Then the image is transformed from greyscale to binary image using an intensity threshold. The selection of an appropriate threshold is crucial, given that a lot of information can be lost or distorted in this step. Once the binary image is obtained a thinning process called "skeletonisation" is applied,

consisting of the conversion of the fringes into thin lines of 1 pixel wide. The skeletonised pixel-based image is first transformed into a vectorial image and then each fringe can be analysed individually in relation to its neighbours.

The "lattice-fringe" analysis performed in this paper contains the following steps for image processing: 1- Region of interest selection, 2- Contrast enhancement using histogram equalisation (discrete gray levels: 5), 3- Gaussian low-pass filter (size 7, sigma 2), 4- Bottom-hat transformation (disk, size 2), 5- Binarisation using Otsu's method, 6- Skeletonisation, 7- Elimination of isolated pixels and pixels with more than 3 connections.

Once the skeleton of the binary image is defined, the connectivity of all pixels is obtained. All connected pixels are detected and stored representing the fringes. The fringe length is then calculated as the Euclidean distance between the fringe pixels. All fringes shorter than 0.483 nm (two aromatic rings) are eliminated as they are non-physical. Due to image manipulation some information can be lost or modified. For example, branched fringes were artificially separated such that they were individual, this could cause a reduction in the length values determined. This should be taken into account in the analysis of the results.

3 Results and Discussion

3.1 Soot volume fraction (F_v)

The large difference in sooting tendency between toluene and heptane flames can be quantified through **Equation 1**, which calculates the F_v , from the experimentally determined radially distributed extinction profile (I/I_0) [61].

$$F_v = \frac{-\ln\left(\frac{I}{I_0}\right)\lambda}{lK_e} \quad (1)$$

where l is the path length (tomographic reconstruction step size, 0.05 cm, for this application), λ is the wavelength of light, and K_e is the dimensionless extinction coefficient of soot. The value for the dimensionless extinction coefficient of soot has been studied and characterised in a variety of fuel systems [34, 35, 58]. *Krishnan et al.* studied the effect of liquid and gaseous fuels across a range of molecular weights on K_e finding a relatively consistent value of 8.6 ± 1.5 at 514.5 nm, which is used in this work [35]. The errors in reported F_v measurements are calculated from the uncertainty in replicate extinction measurements, but the uncertainty in K_e value results in a 20% error intrinsic to reported F_v values.

Figure 2 presents an image of the calculated F_v for the heptane, H50T50 and toluene flames measured at 540 nm. In the heptane flame particle concentrations were not observable until 1 cm HAB (in the wings) and 2.5 cm HAB (in the centerline) and maximum soot concentrations are found in the centre of the flame. As toluene is added the maximum concentration migrates from the centre to the wings, a similar trend has been observed in other highly sooting flames [1]. The maximum F_v concentration in H50T50 and toluene flames exceed the maximum heptane F_v by a factor of four.

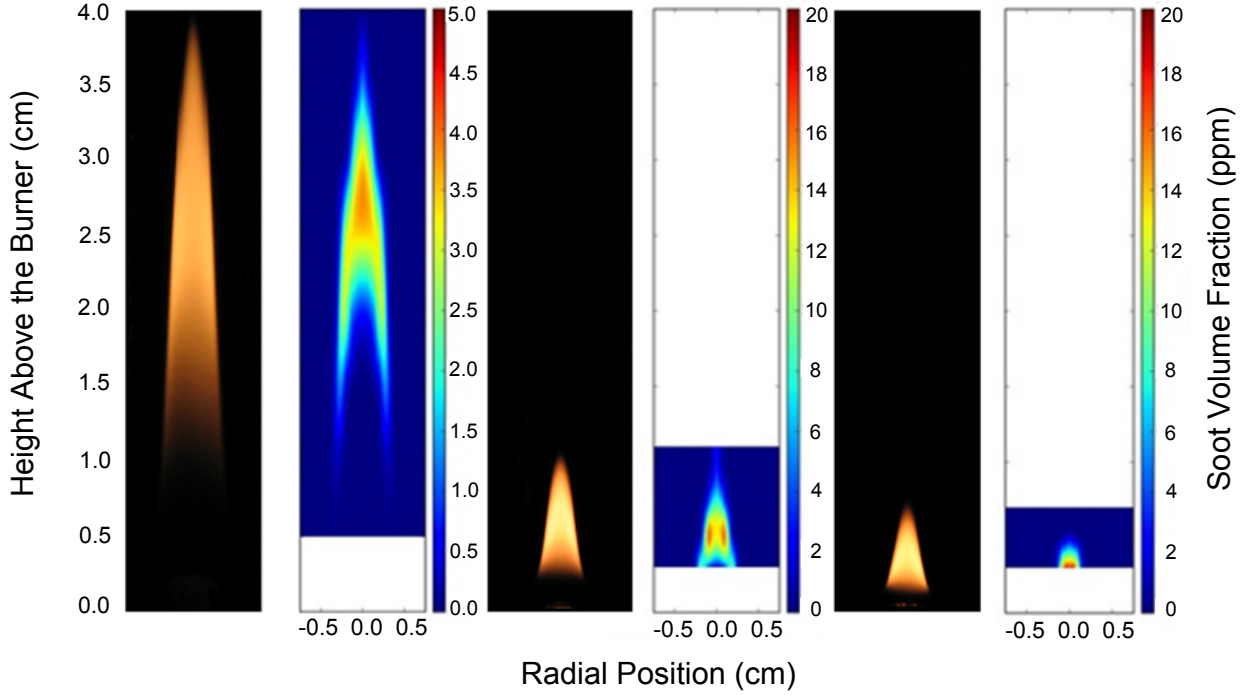


Figure 2: F_v as calculated from extinction measurements at 540 nm. Left: heptane flame (peak F_v 3.8 ppm \pm 0.5 ppm); Centre: H50T50 flame (peak F_v 16.2 ppm \pm 2.7 ppm); Right: toluene flame (peak F_v 18.0 ppm \pm 0.6 ppm).

3.2 OBG calculation

In the late 1960's and early 1970's, two groups (Tauc and Davis/Mott) demonstrated that the long wavelength edge of the optical absorption of amorphous semiconductors acts as a probe of the localised states [52, 59]. Therefore the optical band gap (OBG) can be calculated from **Equation 2**.

$$h\nu \cdot \alpha \approx (h\nu - OBG)^r \quad (2)$$

where α is the extinction coefficient and r is a constant describing the directness and quantum mechanical allowedness of the optical transition. In this work a value of $r=0.5$ is used corresponding to a direct allowed transition [19, 41]. A more detailed discussion for choice of r value and the methodology followed in this work can be found in a recent publication by Adkins and Miller [1]. To determine the OBG, $(h\nu \cdot \alpha)^{1/r}$ was plotted as a function of photon energy (eV), and the straight line portion (determined in previous publications to be over the spectral range from 440 nm to 540 nm [1]) of the plot was extrapolated to the x -intercept. This procedure was repeated at each height and radial position, only using position data where the linear portion possessed an R^2 greater than 0.9 and where the exponential fit noise was less than 50%.

In the heptane flame (**Figure 3a**) it can be observed that at low HAB, OBG is lower close to the flame front, where there is the largest concentration of soot. Moving downstream,

to the tip of the flame, lower values of OBG are found close to the flame centerline. The same behaviour is observed in H50T50 and toluene flames (**Figures 3b,3c**). At the tip of the flames there was not sufficient soot for a reliable estimation of OBG, except in the toluene flame. At the tip of this flame the OBG is larger due to oxidation of the particles as they approach the tip. Oxidation at the tip has been observed in similar flame systems using different diagnostics [9].

3.3 Correlating OBG Measurements to Molecular size

Robertson and Ferrari showed that systems with sp² character, such as soot, have electronic properties that are dominated by $\pi - \pi^*$ interactions [46, 47]. Based on these conclusions, they showed the OBG scales inversely with the size of the pericondensed aromatic structure [11, 23, 24]. Using this relationship, *Miller et al.* related computational results of the calculated HOMO-LUMO gaps for a variety of D_{2h} PAH molecules to the number of aromatic rings in the structure resulting in the following relationship (**Equation 3**):

$$OBG = \frac{5.8076}{M^{1/2}} + 0.5413 = \frac{1.4787}{L_a} + 0.5413 \quad (3)$$

where M is the number of aromatic rings and L_a is the conjugation length [46, 47]. In different techniques various titles for the variable L_a have been used including “in-plane crystallite size”, “correlation length”, and “conjugation length”. All of these descriptors address the same concept of the characteristic dimension of a planar π system. **Figure 4** combines the relationship between the number of aromatic rings and the OBG and the relationship between the number of aromatic rings and the conjugation length to relate the experimentally determined OBG to the physical size of the PAH [38]. The grey bands correspond to the range of experimentally determined OBG in the n-heptane flame correlated with the number of aromatic rings and conjugation length.

Throughout the flame systems we observe a fairly consistent range of OBG values in the range of 1.82 - 2.34 (and thus estimated size of PAH of 10-20 rings). The average OBG for the flame systems were 2.06 eV, 1.99 eV, and 2.05 eV for the n-heptane flame, H50T50 flame, and toluene flame, respectively (full summary in **Table 1**). These values correspond to an average aromatic size of something with between 15-16 aromatic rings, about the size of circumpylene. Interestingly, the H50T50 flame has an average OBG lower than either of the component compounds. However, the range in the OBG reported in all flame systems are all within the uncertainty in the measurements.

3.4 Fringe length calculation

Figure 5 show representative HRTEM images of samples taken at the tip of each flame (4 cm HAB for heptane, 1.1 cm HAB for H50T50 and 0.7 cm HAB for toluene). The corresponding image analysis mapping all relevant fringes are presented in the bottom row. An ‘onion-like’ distribution of the fringes is observed, showing nearly spherical

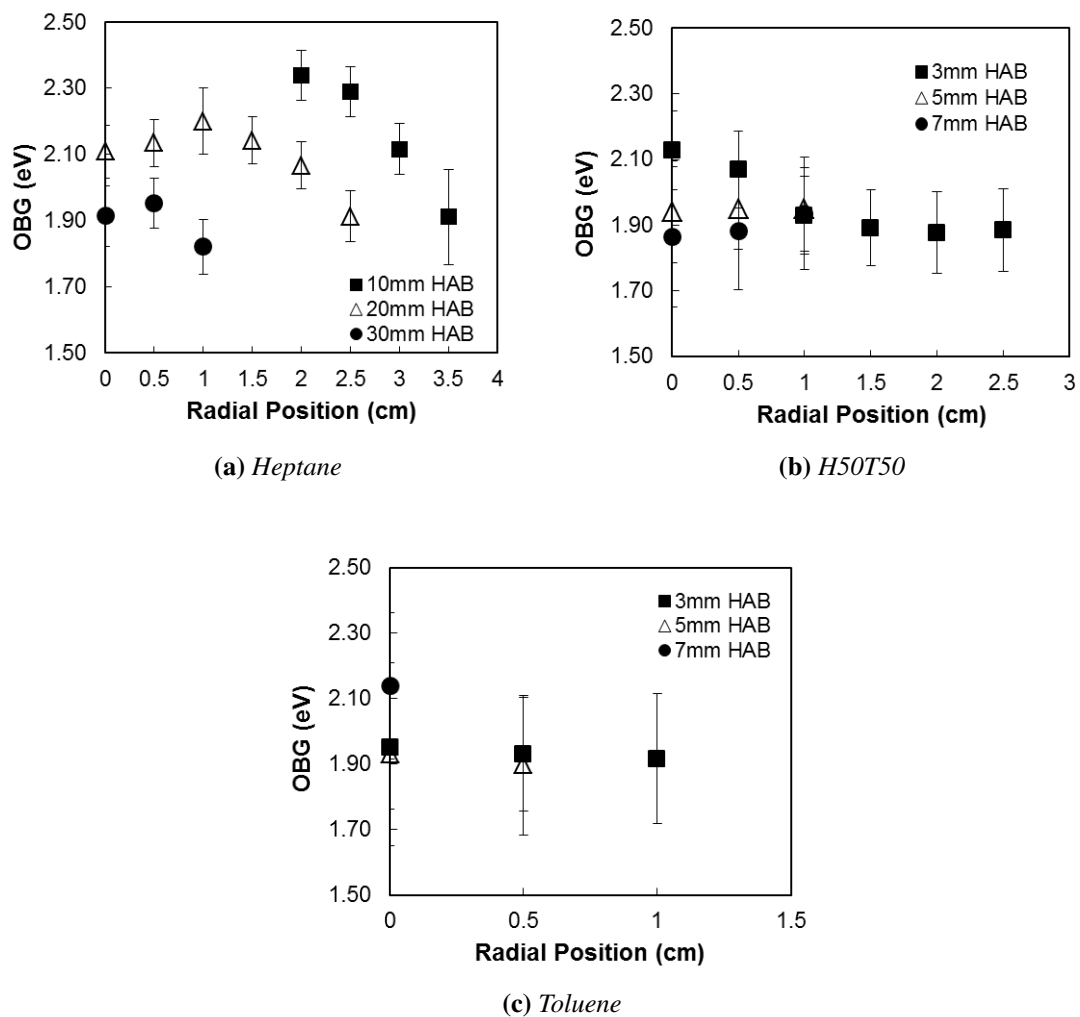


Figure 3: Experimentally determined OBG as a function of radial position and height above the burner for the a) heptane flame, b) 50% heptane-50% toluene flame and c) toluene flame

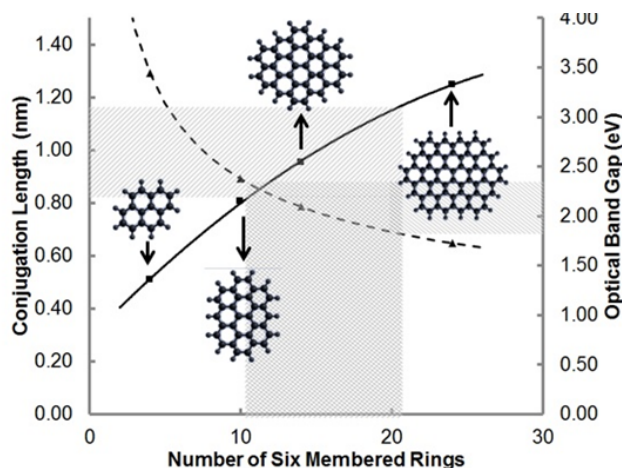


Figure 4: Comparison between calculated HOMO-LUMO energy gaps (OBG) with number of aromatic rings and conjugation length in the *n*-heptane flame. The dashed line and triangle show the relationship between OBG and number of rings. The solid line and squares show the relationship between conjugation length and number of rings. The grey bands depict the range of OBG observed throughout the flame.

primary particles of different sizes stick to each other. Qualitatively heptane's soot seems to have shorter and more curved fringes compared to H50T50 and toluene, indicating a lower degree of graphitisation.

From the lattice-fringe analysis a fringe length distribution is obtained. The mean fringe length calculated at all sampling points for the three flames is presented in **Figure 6**. Results show that the fringe length increases with HAB in the heptane flame, until a point after which it decreases considerably. Previous measurements of soot particle size [7] indicate that oxidation plays a large role and that could explain the smaller fringe length. There is not a significant difference in the mean fringe length obtained in the centerline and the wing at the same HAB. For H50T50 the mean fringe length decreases from 0.7 cm to 1.1 cm HAB, possibly due to oxidation at the flame tip. Toluene was only sampled at the tip and exhibited the highest values of fringe length.

3.5 Comparison of fringe and conjugation length

Table 1 presents the comparison between values of fringe and conjugation lengths, which are both measures of the typical length scale of a PAH. For all fuels the values obtained with the two experimental methodologies are very consistent. Fringe lengths obtained from HRTEM images represent only carbon atoms parallel to the beam, and do not give any information on the 2D-structure of the PAH. The quality of the image is important for the final result.

The results obtained are in agreement with recent studies of conjugation length from both OBG determination and Raman [30] studies conducted using an ethylene-diluted co-flow diffusion flame, where results indicated PAH species with conjugation lengths between

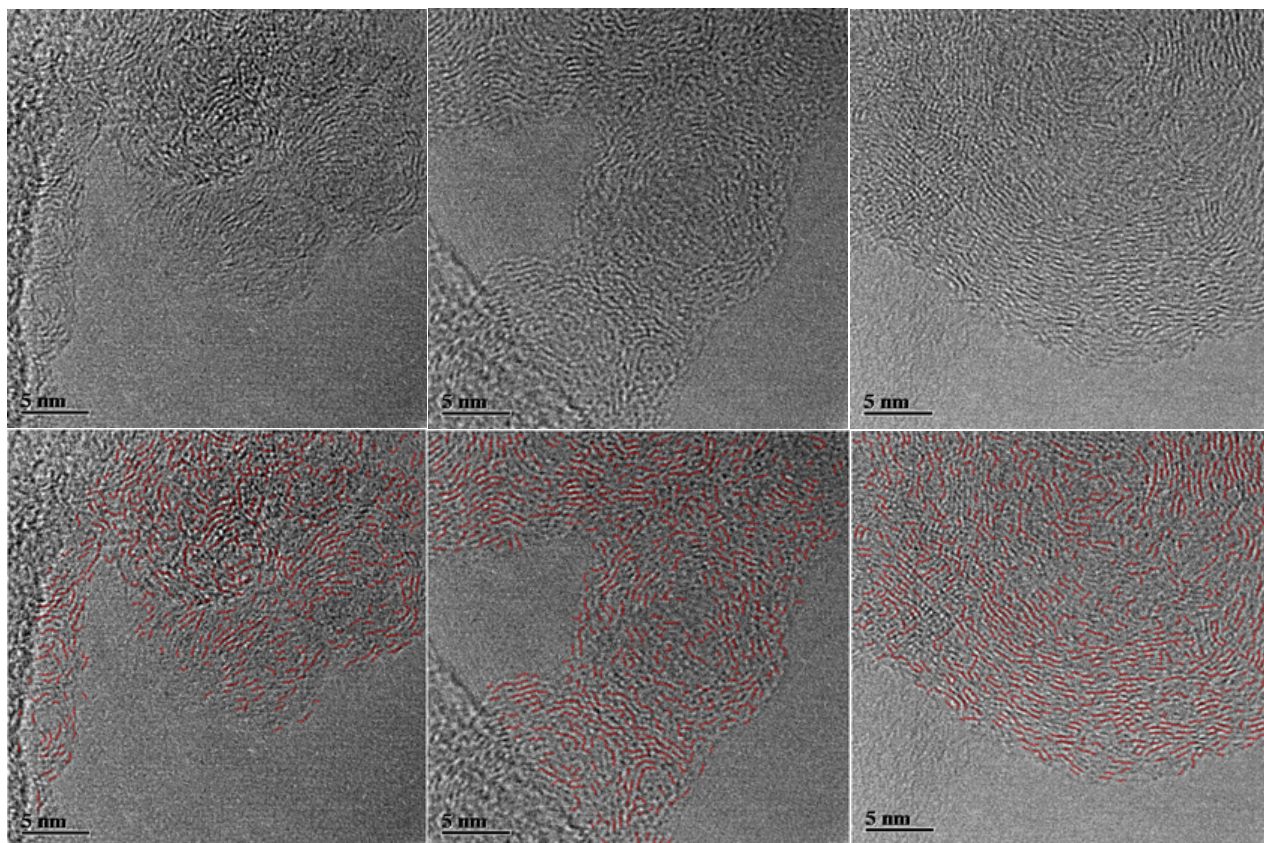


Figure 5: HRTEM images taken at magnification 600,000x, sampled at the tip of the flames. Left: Heptane Flame, Centre: H50T50 Flame, Right: Toluene Flame. Top row corresponds to raw image and bottom row contains overlaid fringe mapping.

0.81 nm to 1.13 nm and 1.0 nm to 1.2 nm, respectively [1, 30]. Similarly, a recent publication of HRTEM in an ethylene flame reports fringe length measurements in the range from 0.94 nm to 1.24 nm and conjugation lengths from Raman studies from 1.03 nm to 1.13 nm [4]. In computational studies we have found a critical size of peri-condensed PAH for mature soot particles in the range of circumcoronene (conjugation length about 1.11 nm) [17].

4 Conclusions

Analysis of extinction measurements and HRTEM was used to estimate the length of molecules that constitute soot particles formed in wick-fed diffusion flames of heptane, toluene and its iso-volumetric mixture. The two estimators are conjugation length obtained from extinction measurements and fringe length derived from HRTEM images. The tomographically reconstructed extinction data was processed using Tauc/Davis-Mott analysis to determine the optical band gap. The OBG ranges from about 1.82 eV to 2.34 eV were measured in the flames correlating to an average size of a structure with 15

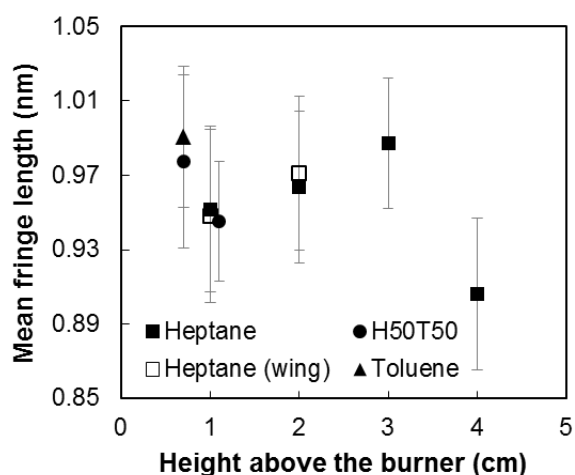


Figure 6: Mean fringe length values calculated from HRTEM images and fringe lattice analysis. Only the heptane flame was sampled at position different than the centerline corresponding to empty symbols. The flame heights are 4 cm for Heptane, 1.1 cm for H50T50 and 0.7 cm for Toluene.

Table 1: Comparison of the range of OBG, conjugation length and fringe length observed across all flame systems.

Flame	OBG (eV)			Number of aromatic rings			Conjugation Length (nm)			Mean fringe length (nm)		
	Min.	Max.	Mean	Min.	Max.	Mean	Min.	Max.	Mean	Min.	Max.	Mean
Heptane	1.82	2.34	2.06	10.4	20.6	15.0	0.82	1.16	0.98	0.91	0.99	0.95
H50T50	1.86	2.17	1.99	12.7	19.4	16.2	0.91	1.12	1.02	0.95	0.98	0.97
Toluene	1.90	2.29	2.05	11.0	18.3	15.3	0.85	1.09	0.99	0.99	0.99	0.99

aromatic rings. Average PAH sizes in the three flames correspond to conjugation lengths between 0.98 nm and 1.02 nm. Similar sizes were obtained using fringe-lattice analysis of HRTEM images taken from soot thermophoretically sampled in the same flames. Mean fringe lengths between 0.95 nm and 0.99 nm were estimated. These results support the theory of soot formation where the transition from chemical to physical growth occurs at modest molecular size; about the size of circumpyrene.

5 Acknowledgments

The authors gratefully acknowledge partial funding by the Royal Society, grant IE120400. This project was partly funded by the National Research Foundation (NRF), Prime Minister's Office, Singapore under its Campus for Research Excellence and Technological Enterprise (CREATE) programme. M.B acknowledges financial support provided by the Administrative Department of Science, Technology and Innovation of Colombia. The GWU portion of this work was supported in part by the U.S. National Science Foundation

under grants CBET-0828950 and CBET-1142284 with Drs Philip Westmoreland, Avind Atreya, and Ruey-Hung Chen serving as technical monitors.

References

- [1] E. M. Adkins and J. H. Miller. Extinction measurements for optical band gap determination of soot in a series of nitrogen-diluted ethylene/air non-premixed flames. *Physical Chemistry Chemical Physics*, 17:2686–2695, 2015. doi:10.1039/C4CP04452E.
- [2] M. Alfe, B. Apicella, R. Barbella, J.-N. Rouzaud, A. Tregrossi, and A. Ciajolo. Structure-property relationship in nanostructures of young and mature soot in pre-mixed flames. *Proceedings of the Combustion Institute*, 32(1):697 – 704, 2009. ISSN 1540-7489. doi:10.1016/j.proci.2008.06.193.
- [3] M. Alfe, B. Apicella, J.-N. Rouzaud, A. Tregrossi, and A. Ciajolo. The effect of temperature on soot properties in premixed methane flames. *Combustion and Flame*, 157(10):1959 – 1965, 2010. ISSN 0010-2180. doi:10.1016/j.combustflame.2010.02.007.
- [4] B. Apicella, P. Pre, M. Alfe, A. Ciajolo, V. Gargiulo, C. Russo, A. Tregrossi, D. Deldique, and J. Rouzaud. Soot nanostructure evolution in premixed flames by high resolution electron transmission microscopy (HRTEM). *Proceedings of the Combustion Institute*, 35(2):1895 – 1902, 2015. ISSN 1540-7489. doi:10.1016/j.proci.2014.06.121.
- [5] J. Appel, H. Bockhorn, and M. Frenklach. Kinetic modeling of soot formation with detailed chemistry and physics: laminar premixed flames of C2 hydrocarbons. *Combustion and Flame*, 121(1-2):122 – 136, 2000. ISSN 0010-2180. doi:10.1016/S0010-2180(99)00135-2.
- [6] ASTM. Standard test method for smoke point of kerosine and aviation turbine fuel. *ASTM Standard D1322-08*, 1997.
- [7] M. L. Botero, S. Mosbach, and M. Kraft. Sooting tendency of paraffin components of diesel and gasoline in diffusion flames. *Fuel*, 126:8 – 15, 2014. ISSN 0016-2361. doi:10.1016/j.fuel.2014.02.005.
- [8] M. L. Botero, D. Chen, S. Gonzáles-Calera, D. Jefferson, and M. Kraft. HRTEM study of soot particles produced by the non-premixed combustion of liquid fuels. *submitted to Carbon*, 2015.
- [9] M. L. Botero, S. Mosbach, J. Akroyd, and M. Kraft. Sooting tendency of surrogates for the aromatic fractions of diesel and gasoline in a wick-fed diffusion flame. *Fuel*, 153:31 – 39, 2015. ISSN 0016-2361. doi:10.1016/j.fuel.2015.02.108.
- [10] H. F. Calcote and D. M. Manos. Effect of molecular structure on incipient soot formation. *Combustion and Flame*, 49(1-3):289–304, 1983. doi:10.1016/0010-2180(83)90172-4.

- [11] L. G. Cançado, K. Takai, T. Enoki, M. Endo, Y. A. Kim, H. Mizusaki, A. Jorio, L. N. Coelho, R. Magalhães-Paniago, and M. A. Pimenta. General equation for the determination of the crystallite size l_a of nanographite by raman spectroscopy. *Applied Physics Letters*, 88(16):163106, 2006. doi:10.1063/1.2196057.
- [12] M. Celnik, R. Patterson, M. Kraft, and W. Wagner. Coupling a stochastic soot population balance to gas-phase chemistry using operator splitting. *Combustion and Flame*, 148(3):158 – 176, 2007. ISSN 0010-2180. doi:10.1016/j.combustflame.2006.10.007.
- [13] M. Celnik, A. Raj, R. West, R. Patterson, and M. Kraft. Aromatic site description of soot particles. *Combustion and Flame*, 155(1 - 2):161 – 180, 2008. ISSN 0010-2180. doi:10.1016/j.combustflame.2008.04.011.
- [14] D. Chen, Z. Zainuddin, E. Yapp, J. Akroyd, S. Mosbach, and M. Kraft. A fully coupled simulation of PAH and soot growth with a population balance model. *Proceedings of the Combustion Institute*, 34(1):1827 – 1835, 2013. ISSN 1540-7489. doi:10.1016/j.proci.2012.06.089.
- [15] D. Chen, T. S. Totton, J. Akroyd, S. Mosbach, and M. Kraft. Phase change of polycyclic aromatic hydrocarbon clusters by mass addition. *Carbon*, 77:25 – 35, 2014. ISSN 0008-6223. doi:10.1016/j.carbon.2014.04.089.
- [16] D. Chen, T. S. Totton, J. W. Akroyd, S. Mosbach, and M. Kraft. Size-dependent melting of polycyclic aromatic hydrocarbon nano-clusters: A molecular dynamics study. *Carbon*, 67:79 – 91, 2014. ISSN 0008-6223. doi:10.1016/j.carbon.2013.09.058.
- [17] D. Chen, J. Akroyd, S. Mosbach, D. Opalka, and M. Kraft. Solid-liquid transitions in homogenous ovalene, hexabenzocoronene and circumcoronene clusters: A molecular dynamics study. *Combustion and Flame*, 162(2):486 – 495, 2015. ISSN 0010-2180. doi:10.1016/j.combustflame.2014.07.025.
- [18] H. Chen and R. Dobbins. Crystallogenesis of particles formed in hydrocarbon combustion. *Combustion Science and Technology*, 159(1):109–128, 2000. doi:10.1080/00102200008935779.
- [19] E. A. Davis and N. F. Mott. Conduction in non-crystalline systems v. conductivity, optical absorption and photoconductivity in amorphous semiconductors. *Philosophical Magazine*, 22(179):0903–0922, 1970. doi:10.1080/14786437008221061.
- [20] R. A. Dobbins and C. M. Megaridis. Morphology of flame-generated soot as determined by thermophoretic sampling. *Langmuir*, 3(2):254–259, 1987. doi:10.1021/la00074a019.
- [21] P. Elvati and A. Violi. Thermodynamics of poly-aromatic hydrocarbon clustering and the effects of substituted aliphatic chains. *Proceedings of the Combustion Institute*, 34(1):1837 – 1843, 2013. ISSN 1540-7489. doi:10.1016/j.proci.2012.07.030.

- [22] J. T. Farrell, N. Cernansky, F. Dryer, C. K. Law, D. G. Friend, C. Hergart, R. M. McDavid, A. K. Patel, C. J. Mueller, and H. Pitsch. Development of an experimental database and chemical kinetic models for surrogate diesel fuels. *SAE technical paper*, (2007-01-0201), 2007. doi:10.4271/2007-01-0201.
- [23] A. C. Ferrari and J. Robertson. Interpretation of raman spectra of disordered and amorphous carbon. *Physics Review B*, 61:14095–14107, May 2000. doi:10.1103/PhysRevB.61.14095.
- [24] A. C. Ferrari and J. Robertson. Resonant raman spectroscopy of disordered, amorphous, and diamondlike carbon. *Physics Review B*, 64:075414, Jul 2001. doi:10.1103/PhysRevB.64.075414.
- [25] M. Frenklach. Reaction mechanism of soot formation in flames. *Physical Chemistry Chemical Physics*, 4:2028–2037, 2002. doi:10.1039/B110045A.
- [26] M. Frenklach and H. Wang. Detailed modeling of soot particle nucleation and growth. *Symposium (International) on Combustion*, 23(1):1559 – 1566, 1991. ISSN 0082-0784. doi:10.1016/S0082-0784(06)80426-1. Twenty-Third Symposium (International) on Combustion.
- [27] M. Frenklach and H. Wang. Detailed mechanism and modeling of soot particle formation. In H. Bockhorn, editor, *Soot Formation in Combustion*, volume 59 of *Springer Series in Chemical Physics*, pages 165–192. Springer Berlin Heidelberg, 1994. ISBN 978-3-642-85169-8.
- [28] A. Hamins, D. T. Anderson, and J. Houston Miller. Mechanistic studies of toluene destruction in diffusion flames. *Combustion Science and Technology*, 71(4-6):175–195, 1990. doi:10.1080/00102209008951631.
- [29] J. Happold, H.-H. Grotheer, and M. Aigner. Distinction of gaseous soot precursor molecules and soot precursor particles through photoionization mass spectrometry. *Rapid Communications in Mass Spectrometry*, 21(7):1247–1254, 2007. ISSN 1097-0231. doi:10.1002/rcm.2955.
- [30] J. D. Herdman, B. C. Connelly, M. D. Smooke, M. B. Long, and J. H. Miller. A comparison of raman signatures and laser-induced incandescence with direct numerical simulation of soot growth in non-premixed ethylene/air flames. *Carbon*, 49(15): 5298 – 5311, 2011. ISSN 0008-6223. doi:10.1016/j.carbon.2011.07.050.
- [31] R. A. Hunt. Relation of smoke point to molecular structure. *Industrial and Engineering Chemistry*, 45(3):602–606, 1953.
- [32] T. Ishiguro, Y. Takatori, and K. Akihama. Microstructure of diesel soot particles probed by electron microscopy: First observation of inner core and outer shell. *Combustion and Flame*, 108(1-2):231 – 234, 1997. ISSN 0010-2180. doi:10.1016/S0010-2180(96)00206-4.

- [33] U. Koylu, C. McEnally, D. Rosner, and L. Pfefferle. Simultaneous measurements of soot volume fraction and particle size / microstructure in flames using a thermophoretic sampling technique. *Combustion and Flame*, 110(4):494 – 507, 1997. ISSN 0010-2180. doi:10.1016/S0010-2180(97)00089-8.
- [34] S. S. Krishnana, K.-C. Lin, and G. M. Faeth. Extinction and scattering properties of soot emitted from buoyant turbulent diffusion flames. *Journal of Heat Transfer*, 123(2):331–339, 2000. doi:10.1115/1.1350823.
- [35] S. S. Krishnana, K.-C. Lin, and G. M. Faeth. Optical properties in the visible of overfire soot in large buoyant turbulent diffusion flames. *Journal of Heat Transfer*, 122(3):517–524, 2000. doi:10.1115/1.1288025.
- [36] J. S. Lowe, J. Y. Lai, P. Elvati, and A. Violi. Towards a predictive model for polycyclic aromatic hydrocarbon dimerization propensity. *Proceedings of the Combustion Institute*, 35(2):1827 – 1832, 2015. ISSN 1540-7489. doi:10.1016/j.proci.2014.06.142.
- [37] J. H. Miller. Aromatic excimers: evidence for polynuclear aromatic hydrocarbon condensation in flames. *Proceedings of the Combustion Institute*, 30(1):1381 – 1388, 2005. ISSN 1540-7489. doi:10.1016/j.proci.2004.08.192.
- [38] J. H. Miller, J. D. Herdman, C. D. Green, and E. M. Webster. Experimental and computational determinations of optical band gaps for PAH and soot in a N₂-diluted, ethylene/air non-premixed flame. *Proceedings of the Combustion Institute*, 34(2):3669 – 3675, 2013. ISSN 1540-7489. doi:10.1016/j.proci.2012.05.054.
- [39] P. Mitchell and M. Frenklach. Monte carlo simulation of soot aggregation with simultaneous surface growth-why primary particles appear spherical. *Symposium (International) on Combustion*, 27(1):1507 – 1514, 1998. ISSN 0082-0784. doi:10.1016/S0082-0784(98)80558-4. Twenty-Seventh Symposium (International) on Combustion Volume One.
- [40] S. Mosbach, M. S. Celnik, A. Raj, M. Kraft, H. R. Zhang, S. Kubo, and K.-O. Kim. Towards a detailed soot model for internal combustion engines. *Combustion and Flame*, 156(6):1156 – 1165, 2009. ISSN 0010-2180. doi:10.1016/j.combustflame.2009.01.003.
- [41] K. W. Nevill F. Mott, E. A. Davis. *Electronic Processes in Non-Crystalline Materials*. Oxford University Press, 1971.
- [42] W. Pitz, N. Cernansky, F. Dryer, F. Egolfopoulos, J. T. Farrell, D. G. Friend, and H. Pitsch. Development of an experimental database and chemical kinetic models for surrogate gasoline fuels. *SAE technical paper*, (2007-01-0175), 2007. doi:10.4271/2007-01-0175.
- [43] A. Raj, M. Celnik, R. Shirley, M. Sander, R. Patterson, R. West, and M. Kraft. A statistical approach to develop a detailed soot growth model using PAH characteristics. *Combustion and Flame*, 156(4):896 – 913, 2009. ISSN 0010-2180. doi:10.1016/j.combustflame.2009.01.005.

- [44] A. Raj, M. Sander, V. Janardhanan, and M. Kraft. A study on the coagulation of polycyclic aromatic hydrocarbon clusters to determine their collision efficiency. *Combustion and Flame*, 157(3):523 – 534, 2010. ISSN 0010-2180. doi:10.1016/j.combustflame.2009.10.003.
- [45] H. Richter and J. Howard. Formation of polycyclic aromatic hydrocarbons and their growth to soot - a review of chemical reaction pathways. *Progress in Energy and Combustion Science*, 26(4 - 6):565 – 608, 2000. ISSN 0360-1285. doi:10.1016/S0360-1285(00)00009-5.
- [46] J. Robertson. *World of Carbon*, volume 1, chapter Graphite and precursors, pages 249–273. Gordon and Breach, 2001.
- [47] J. Robertson and E. P. O’Reilly. Electronic and atomic structure of amorphous carbon. *Physics Review B*, 35:2946–2957, Feb 1987. doi:10.1103/PhysRevB.35.2946.
- [48] M. Sander, R. I. Patterson, A. Braumann, A. Raj, and M. Kraft. Developing the PAH-PP soot particle model using process informatics and uncertainty propagation. *Proceedings of the Combustion Institute*, 33(1):675 – 683, 2011. ISSN 1540-7489. doi:10.1016/j.proci.2010.06.156.
- [49] R. Schalla and G. McDonald. Variation in smoking tendency among hydrocarbons of low molecular weight. *Industrial and Chemical Chemistry*, 45(7):1497–1500, 1953.
- [50] C. A. Schuetz and M. Frenklach. Nucleation of soot: Molecular dynamics simulations of pyrene dimerization. *Proceedings of the Combustion Institute*, 29(2):2307 – 2314, 2002. ISSN 1540-7489. doi:10.1016/S1540-7489(02)80281-4.
- [51] J. Singh, M. Balthasar, M. Kraft, and W. Wagner. Stochastic modeling of soot particle size and age distributions in laminar premixed flames. *Proceedings of the Combustion Institute*, 30(1):1457 – 1465, 2005. ISSN 1540-7489. doi:10.1016/j.proci.2004.08.120.
- [52] J. Tauc, R. Grigorovici, and A. Vancu. Optical properties and electronic structure of amorphous germanium. *physica status solidi b*, 15(2):627–637, 1966. ISSN 1521-3951. doi:10.1002/pssb.19660150224.
- [53] T. S. Totton, D. Chakrabarti, A. J. Misquitta, M. Sander, D. J. Wales, and M. Kraft. Modelling the internal structure of nascent soot particles. *Combustion and Flame*, 157(5):909 – 914, 2010. ISSN 0010-2180. doi:10.1016/j.combustflame.2009.11.013.
- [54] R. L. V. Wal. A TEM methodology for the study of soot particle structure. *Combustion Science and Technology*, 126(1-6):333–351, 1997. doi:10.1080/00102209708935680.
- [55] R. L. V. Wal. An illustration of soot structure by dark field transmission electron microscopy. *Combustion Science and Technology*, 132(1-6):315–323, 1998. doi:10.1080/00102209808952018.

- [56] H. Wang. Formation of nascent soot and other condensed-phase materials in flames. *Proceedings of the Combustion Institute*, 33(1):41 – 67, 2011. ISSN 1540-7489. doi:10.1016/j.proci.2010.09.009.
- [57] R. J. Watson, M. L. Botero, C. J. Ness, N. M. Morgan, and M. Kraft. An improved methodology for determining threshold sooting indices from smoke point lamps. *Fuel*, 111:120 – 130, 2013. ISSN 0016-2361. doi:10.1016/j.fuel.2013.04.024.
- [58] T. Williams, C. Shaddix, K. Jensen, and J. Suo-Anttila. Measurement of the dimensionless extinction coefficient of soot within laminar diffusion flames. *International Journal of Heat and Mass Transfer*, 50(7 - 8):1616 – 1630, 2007. ISSN 0017-9310. doi:10.1016/j.ijheatmasstransfer.2006.08.024.
- [59] D. L. Wood and J. Tauc. Weak absorption tails in amorphous semiconductors. *Physics Review B*, 5:3144–3151, Apr 1972. doi:10.1103/PhysRevB.5.3144.
- [60] K. Yehliu, R. L. V. Wal, and A. L. Boehman. Development of an HRTEM image analysis method to quantify carbon nanostructure. *Combustion and Flame*, 158(9): 1837 – 1851, 2011. ISSN 0010-2180. doi:10.1016/j.combustflame.2011.01.009.
- [61] H. Zhao and N. Ladommatos. Optical diagnostics for soot and temperature measurement in diesel engines. *Progress in Energy and Combustion Science*, 24(3):221 – 255, 1998. ISSN 0360-1285. doi:10.1016/S0360-1285(97)00033-6.